Two-dimensional fluid approach to the dc magnetron discharge

Plasma Sources Sci. Technol. **14** (2005) 168–176 doi:10.1088/0963-0252/14/1/018

Two-dimensional fluid approach to the dc magnetron discharge

C Costin[1,2], L Marques[1,3], G Popa[2] and G Gousset[1]

[1] Laboratoire de Physique des Gaz et des Plasmas, Université Paris Sud XI, Bât. 210, 91405 Orsay Cedex, France
[2] Faculty of Physics, Al. I. Cuza University, 11 Carol I Blvd., 700506 Iasi, Romania
[3] Departamento de Física, Universidade do Minho, 4710-057 Braga, Portugal

E-mail: claudiu@uaic.ro

Received 27 February 2004
Published 1 February 2005
Online at stacks.iop.org/PSST/14/168

Abstract
A two-dimensional (r, z) time-dependent fluid model was developed and used to describe a dc planar magnetron discharge with cylindrical symmetry. The transport description of the charged species uses the corresponding first three moments of the Boltzmann equation: continuity, momentum transfer and mean energy transfer (the last one only for electrons), coupled with the Poisson equation. An original method is proposed to treat the transport equations. Electron and ion momentum transport equations are reduced to the classical drift–diffusion expression for the fluxes since the presence of the magnetic field is introduced as an additional part in the electron flux, while for ions an effective electric field was considered. Thus, both continuity and mean energy transfer equations are solved in a classical manner. Numerical simulations were performed considering argon as a buffer gas, with a neutral pressure varying between 5 and 30 mTorr, for different voltages applied on the cathode. Results obtained for densities of the charged particle, fluxes and plasma potential are in good agreement with those obtained in previous studies.

1. Introduction

The magnetron discharge stands out from other low pressure electrical discharges because of the presence of a strongly non-homogeneous magnetic field in front of the cathode (target). In our particular case, this field is created by a pair of magnets co-axially disposed under the cathode plate (figure 1). As a consequence of the geometric arrangement a balanced or unbalanced structure of field lines emerges [1]. A strong axial electric field, $\vec{E}_z$, is present in the magnetic field region due to the cathode fall. The simultaneous action of these two fields leads to a high density confined plasma, which permits a low voltage operating discharge (hundreds of volts) at very low pressures, typically about 10 mTorr. The Larmor radius for ions is of the order of centimetres, while the thickness of the cathode fall does not exceed a few millimetres. Thus, the ions might be considered as not being affected by the magnetic field but accelerated directly to the cathode, where by impact on the surface they are able to generate secondary electrons and to sputter particles that can typically be used for surface deposition of a wafer placed in front of the target.

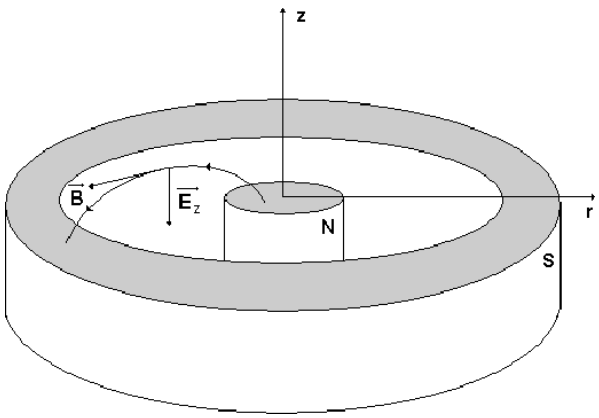

Figure 1. Magnet configuration.

Magnetron discharges were and still are extensively studied experimentally, analytically or numerically in order to better understand both the physical and chemical processes involved in their multiple applications. Working in pure rare

gases [2–5, 9] or reactive mixtures [5–8], in dc [7–9], RF [5, 6] or pulsed regimes [2–4], magnetron discharges are mainly (and widely) used as sputter/deposition sources.

Over the last few years, many numerical models were proposed to properly describe these discharges and to speed up the computing time. Particle-in-cell/Monte Carlo collision (PIC-MCC) is a very common technique applied for two-dimensional [10–12] or three-dimensional [13] simulations. It is easy to implement, without *a priori* physical approximations except that of the classical nature of particle trajectories, and is very useful for non-equilibrium processes, but it requires a very large amount of computational time. The hybrid model combines the particle and continuum models, achieving more reasonable computing times. In some studies [1, 14] fast electrons, such as secondary emitted electrons at the cathode, which are accelerated in the cathode fall (mainly giving the ionization rate), are treated by the Monte Carlo model, while for slow electrons and ions, which are the dominant particle population, the fluid equations are used. Other authors [15] combine a particle simulation of neutral atoms and ions with a fluid description of electrons. Here, such a model is applied to stationary plasma thrusters (SPT), devices related to magnetron discharges through the presence of a magnetic field. In the kinetic model [16, 17] a microscopic description of the plasma is carried out. The distribution functions of the particles are calculated by solving the Boltzmann equation and the macroscopic plasma parameters can be obtained by integrating over the distribution functions. The kinetic model is often combined with a collisional–radiative one [18, 19], which requires us to solve rate balance equations for excited species.

Despite numerous papers devoted to the modelling of this type of discharge, those using the fluid approach are very rare and, more often, a one-dimensional treatment of fluid equations is done [20, 21]. This is mainly due to the difficulty in treating the effect of the inhomogeneous magnetic field on the electrons. The problem is typically three-dimensional but it can be spatially reduced to two dimensions in the particular case of cylindrical symmetry. For numerical simulations the fluid model has an advantage in terms of the computing time but it loses validity with decrease in the gas pressure when the mean free path of charged particles strongly exceeds the characteristic length of the discharge. Although magnetron discharges work at low pressures (1 to tens of mTorr), the presence of the magnetic field reduces the effective distance covered by electrons between two collisions, which is equivalent to an increase of the pressure, thus fulfilling the hydrodynamic hypothesis. As an alternative point of view, the set of fluid equations considered in this work should be regarded as a pure macroscopic representation of the electron Boltzmann equation whose solution mainly concerns the calculation of the electron density and mean energy. Such a quantity plays a crucial role in defining a spatial dependence for the electron distribution function, when adopting the *local mean energy approximation* as in this work. We must pay attention to the fact that, due to the large electron density, the Boltzmann equation can still describe the electron kinetics and, consequently, we can suppose this is also true for its moments.

This paper presents an original two-dimensional (r, z), time-dependent fluid model approach to describe the transport

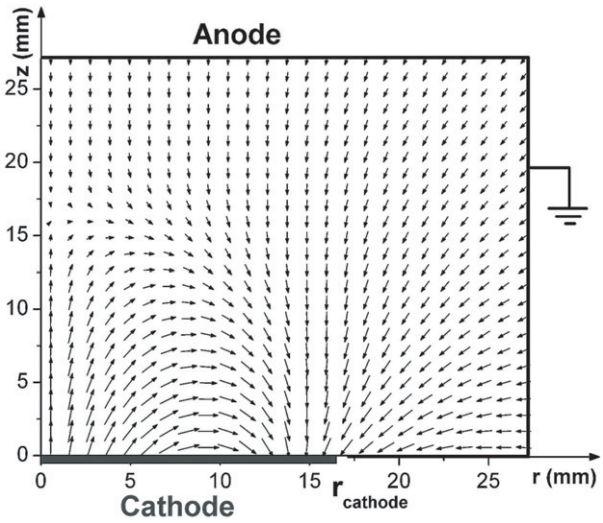

Figure 2. Reactor geometry and magnetic field map.

of two charged species, electrons and positive ions, in a cylindrically symmetric dc planar magnetron reactor. The transport of the charged species is described by the corresponding first three moments of the Boltzmann equation—continuity, momentum transfer and mean energy transfer equation (the last only for electrons)—coupled with the Poisson equation. Due to the strong coupling of the fluid equations in the presence of the magnetic field, some assumptions are required in order to simplify the numerical procedure. Thus, all transport equations are treated in the same manner, using a classical drift–diffusion expression for fluxes. This condition is achieved by introducing the influence of the magnetic field as an additional part in the electron flux and considering an effective electric field for ions. Boundary conditions are set for the fluxes of the charged particles and for the electric potential at the walls.

Computations were performed for a planar magnetron device, schematically drawn in figure 2. Argon was chosen as the working gas. Due to the cylindrical symmetry of the system only a bi-dimensional picture is plotted. The cathode is a metallic disc, with radius $r_{\mathrm{cath}} = 16.5\,\mathrm{mm}$, and grounded metallic walls playing the role of the anode ($R_{\max} = Z_{\max} = 26.95\,\mathrm{mm}$). The neutral gas pressure varies between 5 and 30 mTorr, for a gas temperature of 350 K. The applied dc voltages on the cathode are -350 and -550 V. The magnetic field structure is unbalanced, as shown in figure 2. For convenient visualization, the length of the plotted vectors is made proportional to the logarithm of the magnetic field strength, $\ln B$, measured and numerically fitted as presented in [22]. In the region where the field lines are parallel to the cathode ($r \approx 9.5\,\mathrm{mm}$), the magnetic field strength decreases from about 750 G at $z = 0$, to 20 G at $z \approx 15\,\mathrm{mm}$. Several plasma parameters, such as the plasma potential, densities of the charged particles and ion flux at the cathode, are obtained from the model and they are discussed as representative results.

2. Model equations

A two-component fluid model was considered in order to describe the magnetron discharge. The basic fluid equations

were written for electrons (1*a*)–(1*c*) and ions (1*a*) and (1*b*). They consist of the first three moments of the Boltzmann equation, continuity (1*a*), momentum transfer (1*b*) and mean energy transfer (1*c*):

$$\frac{\partial n_\mathrm{s}}{\partial t} + \nabla \cdot \vec{\Gamma}_\mathrm{s} = S, \tag{1a}$$

$$m_\mathrm{s} n_\mathrm{s} \left[\frac{\partial \vec{v}_\mathrm{s}}{\partial t} + (\vec{v}_\mathrm{s} \cdot \nabla)\vec{v}_\mathrm{s} \right] = q_\mathrm{s} n_\mathrm{s} (\vec{E} + \vec{v}_\mathrm{s} \times \vec{B}) - \nabla \vec{\vec{P}}_\mathrm{s} - m_\mathrm{s} n_\mathrm{s} f_\mathrm{ms} \vec{v}_\mathrm{s} \left(1 + \frac{n_\mathrm{e} f_\mathrm{iz}}{n_\mathrm{s} f_\mathrm{ms}} \right), \tag{1b}$$

$$\frac{\partial (n_\mathrm{e} \varepsilon_\mathrm{e})}{\partial t} + \nabla \cdot \vec{\Gamma}_{\varepsilon \mathrm{e}} = -\vec{\Gamma}_\mathrm{e} \cdot \vec{E} - \theta_\mathrm{e} n_\mathrm{e}, \tag{1c}$$

where s is the type of particle (s = e for electron and i for ion, respectively), n_s the density, m_s the mass, $\vec{v}_\mathrm{s}$ the velocity of the fluid particle, f_iz the ionization frequency by electron–neutral impact, f_ms the total momentum transfer frequency for s-species–neutral collisions, $\vec{E}$ the electric field intensity, $\vec{B}$ the magnetic field strength, $\vec{\vec{P}}_\mathrm{s}$ the pressure tensor, q_s the particle charge, t the time, ε_e the electron mean energy (in eV), θ_e the energy loss rate for electron–neutral collisions, $\vec{\Gamma}_\mathrm{s} = n_\mathrm{s} \vec{v}_\mathrm{s}$ is the flux of particles and $\vec{\Gamma}_{\varepsilon \mathrm{e}} = n_\mathrm{e} \langle \varepsilon_\mathrm{e} \vec{v}_\mathrm{e} \rangle$ the energy flux for electrons. Considering that both electrons and ions are created only by electron–neutral ionization collisions, the source term in the continuity equation is $S = f_\mathrm{iz} n_\mathrm{e}$. The magnetic field, $\vec{B}$, considered in the calculations takes into account only the stationary magnetic field produced by the magnets behind the cathode, excluding the one generated by movement of the charged species. In particular, the azimuthal drift current in the plasma ring in front of the target can be of the order of a few amperes [23]. The magnetic field generated by such currents can be estimated to be about a few per cent of the static field when the latter is of the order of hundreds of Gauss. The electric field and plasma potential are given by the Poisson equation:

$$\Delta V = -\frac{e}{\varepsilon_0}(n_\mathrm{i} - n_\mathrm{e}), \tag{2}$$

$$\vec{E} = -\nabla V. \tag{3}$$

All equations are written in cylindrical coordinates (r, φ, z). Due to axial symmetry of the magnetron, the electric and magnetic fields have no azimuthal components, but the presence of the $\vec{E} \times \vec{B}$ drift generates a flux component, $\Gamma_{s\varphi}$, in the φ direction. However, disregarding the possible drift current instabilities, this component can be expressed as a function of Γ_{sr} and Γ_{sz}, thus, permitting us to reduce the problem to a bi-dimensional one, (r, z).

3. Electron transport treatment

Starting from the momentum transfer equation (1*b*), the electron flux can be expressed in the form

$$\vec{\Gamma}_\mathrm{e} = \vec{\Gamma}_\mathrm{e}^0 + \vec{\Gamma}_\mathrm{e}^1 \tag{4}$$

with $\vec{\Gamma}_\mathrm{e}^0$ the classical drift–diffusion flux and $\vec{\Gamma}_\mathrm{e}^1$ a contribution of the magnetic field. To obtain (4) some simplifying assumptions were made in equation (1*b*): (i) the inertial term $m_\mathrm{e} n_\mathrm{e} [\partial \vec{v}_\mathrm{e}/\partial t + (\vec{v}_\mathrm{e} \cdot \nabla)\vec{v}_\mathrm{e}]$ was neglected due to the small mass of the electron; (ii) the ionization frequency f_iz was also neglected with respect to the total electron–neutral momentum transfer frequency, f_me; (iii) considering an isotropic electron distribution function, the pressure tensor becomes a scalar, $P_\mathrm{e} = n_\mathrm{e} k T_\mathrm{e}$. Thus, the momentum transfer equation can be written as

$$n_\mathrm{e} \vec{v}_\mathrm{e} = -\frac{e}{m_\mathrm{e} f_\mathrm{me}} n_\mathrm{e} \vec{E} - \nabla \left(\frac{k T_\mathrm{e}}{m_\mathrm{e} f_\mathrm{me}} n_\mathrm{e} \right) - \frac{e}{m_\mathrm{e} f_\mathrm{me}} n_\mathrm{e} \vec{v}_\mathrm{e} \times \vec{B}, \tag{5}$$

where $\mu_\mathrm{e} = e/m_\mathrm{e} f_\mathrm{me}$ and $D_\mathrm{e} = k T_\mathrm{e}/m_\mathrm{e} f_\mathrm{me}$ are the electron mobility and diffusion coefficient, respectively. The two electron flux components are then

$$\vec{\Gamma}_\mathrm{e}^0 = -\mu_\mathrm{e} n_\mathrm{e} \vec{E} - \nabla (D_\mathrm{e} n_\mathrm{e}) \tag{6a}$$

and

$$\vec{\Gamma}_\mathrm{e}^1 = -n_\mathrm{e} \vec{v}_\mathrm{e} \times \frac{\vec{\Omega}_\mathrm{e}}{f_\mathrm{me}} \equiv -\vec{\Gamma}_\mathrm{e} \times \frac{\vec{\Omega}_\mathrm{e}}{f_\mathrm{me}}, \tag{6b}$$

where $\vec{\Omega}_\mathrm{e} = e\vec{B}/m_\mathrm{e}$ is related to the electron cyclotron gyrofrequency. Due to the cylindrical symmetry $\vec{\Gamma}_\mathrm{e}^0$ has only two components, Γ_{er}^0 and Γ_{ez}^0, while $\vec{\Gamma}_\mathrm{e}^1$ has also the azimuthal one induced by the magnetic field:

$$\begin{pmatrix} \Gamma_{er}^1 \\ \Gamma_{e\varphi}^1 \\ \Gamma_{ez}^1 \end{pmatrix} = \frac{1}{f_\mathrm{me}^2 + \Omega_\mathrm{e}^2} \begin{pmatrix} -\Omega_{ez}^2 & \Omega_{er}\Omega_{ez} \\ f_\mathrm{me}\Omega_{ez} & -f_\mathrm{me}\Omega_{er} \\ \Omega_{er}\Omega_{ez} & -\Omega_{er}^2 \end{pmatrix} \begin{pmatrix} \Gamma_{er}^0 \\ \Gamma_{ez}^0 \end{pmatrix}. \tag{7a}$$

The azimuthal flux component $\Gamma_{e\varphi}$ can be deduced from the combination of equations (4) and (7*a*), as a function of Γ_{er} and Γ_{ez}

$$\Gamma_{e\varphi} = \frac{1}{f_\mathrm{me}} (\Gamma_{er}\Omega_{ez} - \Gamma_{ez}\Omega_{er}). \tag{7b}$$

The reduced electron transport parameters, $D_\mathrm{e}N$ and $\mu_\mathrm{e}N$, depend on the electron energy distribution function (EEDF), $f(\vec{r}, u)$, where $u = m_\mathrm{e} v^2/2e$ is the electron kinetic energy in eV. Under the classical two terms approximation of the EEDF they can be written [24] as

$$D_\mathrm{e}(\vec{r})N = \frac{1}{3}\sqrt{\frac{2e}{m_\mathrm{e}}} \int_0^\infty \frac{u}{\sigma_\mathrm{me}(u)} f_0(\vec{r}, u) \mathrm{d}u, \tag{8a}$$

$$\mu_\mathrm{e}(\vec{r})N = -\frac{1}{3}\sqrt{\frac{2e}{m_\mathrm{e}}} \int_0^\infty \frac{u}{\sigma_\mathrm{me}(u)} \frac{\partial f_0(\vec{r}, u)}{\partial u} \mathrm{d}u, \tag{8b}$$

where σ_me is the total electron–neutral momentum transfer collision cross section, N is the gas density and $f_0(\vec{r}, u)$ is the isotropic part of $f(\vec{r}, u)$, satisfying the normalization condition $\int_0^\infty f_0(\vec{r}, u) u^{1/2} \mathrm{d}u = 1$.

The energy flux is written in the same manner as the particle flux, with corresponding reduced transport coefficients, $D_{\varepsilon\mathrm{e}}N$ and $\mu_{\varepsilon\mathrm{e}}N$ [24]:

$$D_{\varepsilon\mathrm{e}}(\vec{r})N = \frac{1}{\varepsilon_\mathrm{e}(\vec{r})} \frac{1}{3}\sqrt{\frac{2e}{m_\mathrm{e}}} \int_0^\infty \frac{u^2}{\sigma_\mathrm{me}(u)} f_0(\vec{r}, u) \mathrm{d}u, \tag{8c}$$

$$\mu_{\varepsilon\mathrm{e}}(\vec{r})N = -\frac{1}{\varepsilon_\mathrm{e}(\vec{r})} \frac{1}{3}\sqrt{\frac{2e}{m_\mathrm{e}}} \int_0^\infty \frac{u^2}{\sigma_\mathrm{me}(u)} \frac{\partial f_0(\vec{r}, u)}{\partial u} \mathrm{d}u. \tag{8d}$$

The spatial map of electron transport parameters can be obtained by adopting the local mean energy approximation [24], which involves introducing the spatial dependence of EEDF via the electron mean energy profile, $\varepsilon_e(\vec{r})$. The profile $\varepsilon_e(\vec{r})$ of the electron mean energy is obtained as a solution of the electron mean energy transfer equation (1c). Instead of calculating the solution of the electron Boltzmann equation, a Maxwellian EEDF was considered:

$$f_0(\vec{r}, u) = f_0[\varepsilon_e(\vec{r}), u] \equiv \frac{2}{\sqrt{\pi}} \left[\frac{2\varepsilon_e(\vec{r})}{3}\right]^{-3/2} e^{-3u/2\varepsilon_e(\vec{r})}. \quad (9)$$

The validity of this assumption will be discussed in section 7. In equation (1c), electron energy loss rate in elastic and inelastic (excitation, ionization) collisions is calculated according to [24]

$$\theta_e(\vec{r}) = N\frac{2m_e}{M_n}\sqrt{\frac{2e}{m_e}}\int_0^\infty \sigma_{e-n}^{el}(u) f_0(\vec{r}, u) u^2 \, du + \sum_k^{inel} W_k f_{ke}(\vec{r}), \quad (10)$$

where M_n is the mass of neutral atoms, σ_{e-n}^{el} is the elastic cross section of the electron–neutral collision, W_k the energetic threshold for the k-inelastic process characterized by f_{ke}, the collision frequency. All collision frequencies are calculated with

$$f_{ke}(\vec{r}) = N\sqrt{\frac{2e}{m_e}}\int_0^\infty \sigma_{ke}(u) f_0(\vec{r}, u) u \, du, \quad (11)$$

using the collision cross sections given in [25]. Elastic, excitation and ionization collisions with ground state neutrals are considered.

4. Ion transport treatment

In the ion momentum transfer equation, the inertial term cannot be neglected due to the heavier mass of the ion. The influence of the magnetic field was not considered because the ion cyclotron gyro-radius is larger than the linear dimension of the examined region. In front of the cathode, where the magnetic field is important, the ion Larmor radius is larger than 7 cm, while the linear dimension of the examined region is 2.7 cm. Under such assumptions, the ion momentum transfer equation becomes

$$n_i\vec{v}_i = \frac{e}{m_i f_{mi}} n_i \vec{E} - \nabla\left(\frac{kT_i}{m_i f_{mi}} n_i\right) - \frac{n_e f_{iz}}{n_i f_{mi}} n_i \vec{v}_i - \frac{1}{f_{mi}} n_i \left[\frac{\partial \vec{v}_i}{\partial t} + (\vec{v}_i \cdot \nabla)\vec{v}_i\right], \quad (12)$$

where the ion pressure was also taken to be a scalar, $P_i = n_i k T_i$. This last assumption is justified even in the cathode fall where a strong electric field is present. In this region, the main movement of the ions is the drift one. Superposed on this movement is also the thermal one, characterized by a Maxwellian distribution function. The drift movement gives the velocity of the ion fluid particle while the thermal movement is responsible for the diffusion. Their separation in expression (12) allows the use of a scalar pressure. For convenience, the ion flux is written in a drift–diffusion form by introducing an effective electric field, $\vec{E}^{eff}$, [26] as

$$\vec{\Gamma}_i = n_i\vec{v}_i \equiv \mu_i n_i \vec{E}^{eff} - \nabla(D_i n_i). \quad (13)$$

Identifying these two expressions, (12) and (13), for the ion flux and performing some simple calculations [27], an equation for the space–time evolution of $\vec{E}^{eff}$ is obtained:

$$\frac{\partial \vec{E}^{eff}}{\partial t} = f_{mi}(\vec{E} - \vec{E}^{eff}) - f_{iz}\frac{n_e}{n_i}\frac{\vec{v}_i}{\mu_i} - \frac{1}{\mu_i}(\vec{v}_i \cdot \nabla)\vec{v}_i. \quad (14)$$

The reduced diffusion coefficient of argon ions is deduced from the Einstein relation

$$D_i N = \mu_i N \frac{kT_i}{e}, \quad (15)$$

where the ion reduced mobility depends on the reduced effective electric field, $\mu_i N = f(E^{eff}/N)$. The data adopted for this dependence are given in [28] for E/N in the range (0–2) $\times 10^3$ Td and were extrapolated up to 10^5 Td according to [29]. Argon ions were supposed to be thermalized at the gas temperature, $T_i = T_{Ar}$. The ion momentum transfer frequency, f_{mi}, was calculated through the expression for classical mobility

$$f_{mi} = N\frac{e}{m_i(\mu_i N)}. \quad (16)$$

5. Boundary conditions

Fluid equations as well as the Poisson equation can be solved only if boundary conditions are specified. For charged particles, these conditions are imposed on fluxes. All parallel fluxes with respect to any surface are zero, $\Gamma_s^{\parallel} = 0$, s = e, i. In the absence of the magnetic field, the normal electron flux to the anode surface must satisfy $\Gamma_e^{0\perp} = n_e\langle v_e\rangle/2$ [24], where $\langle v_e\rangle$ is the mean electron velocity obtained by integrating over the EEDF. At the cathode, under the same conditions, the normal flux has two components: one comes from the discharge, $n_e\langle v_e\rangle/2$, while the other one is due to the secondary electrons emitted by ion impact, $-\gamma_i\Gamma_i^{\perp}$, where γ_i is the coefficient for secondary electron emission. Due to the very low electron density in the cathode fall—it is 3–4 orders of magnitude lower than the one in the anode sheath—the inner flux is negligible with respect to the flux of the secondary electron emitted, permitting us to write $\Gamma_e^{0\perp} = -\gamma_i\Gamma_i^{\perp}$. Taking into account the magnetic field, the total normal flux is $\Gamma_e^{\perp} = \Gamma_e^{0\perp} + \Gamma_e^{1\perp}$, with $\Gamma_e^{1\perp}$ given by (7a) and $\Gamma_e^{0\parallel}$ zero.

Because the secondary emission coefficient has a strong influence on the properties of the magnetron discharge, some remarks have to be made. Due to the presence of a strong magnetic field close to the cathode surface, the secondary electron trajectory is turned around the field lines, enabling electrons to interact with the target, which reflects or recaptures them. The last process decreases the effective value of the coefficient for total secondary electron emission without a magnetic field, γ_i, so that the magnetron discharge 'sees' only a fraction of it, $\gamma_{net} = \gamma_i(1 - p)$ [30]. As the probability of the recapture, p, depends on both the orientation and magnitude of the magnetic field strength on the cathode surface, from figure 2 it can be concluded that γ_{net} depends on the radial

position, $\gamma_{\rm net}(r) = \gamma_{\rm i}[1 - p(r)]$. Also, it must be mentioned that secondary electrons can collide with gas neutrals or they can interact with the cathode. Once a collision takes place, the electron can no longer return to the surface. Thus, the probability of the recapture depends on the electrons mean free path and, implicitly, on the gas pressure [30]. Even if $\gamma_{\rm net}$ depends on the position, according to [30] a constant coefficient $\gamma_{\rm d}$ can be calculated for the whole cathode surface, as being the effective coefficient 'seen' by the discharge. In our case, it is not necessary to introduce an effective coefficient because it appears explicitly from the calculus; thus, it can also be estimated. Assuming $\Gamma_{\rm e}^{0\perp} = -\gamma_{\rm i}\Gamma_{\rm i}^{\perp}$, the total normal electron flux at the cathode becomes

$$\Gamma_{\rm e}^{\perp} = -\gamma_{\rm i}\Gamma_{\rm i}^{\perp}\left(1 - \frac{\Omega_{er}^2}{f_{\rm me}^2 + \Omega_{\rm e}^2}\right) = -\gamma_{\rm net}\Gamma_{\rm i}^{\perp} \qquad (17)$$

with

$$\gamma_{\rm net} = \gamma_{\rm i}\left(1 - \frac{\Omega_{er}^2}{f_{\rm me}^2 + \Omega_{\rm e}^2}\right). \qquad (18)$$

Expression (18) clearly shows the dependence of $\gamma_{\rm net}$ on the gas pressure, through $f_{\rm me}$, on the magnetic field, through $\Omega_{{\rm e},er}$ and implicitly on the position.

According to [31], below 500 eV, $\gamma_{\rm i}$ can be considered to be independent of the ion energy for clean metal surfaces, with typical values in the range 0.05–0.1. For the Ar–Cu couple, [32] reports a mean value for $\gamma_{\rm i}$ at about 0.01 versus the reduced electric field, E/p, in the range of hundreds of V cm^{-1} Torr^{-1}. In this paper, we chose for $\gamma_{\rm i}$ an intermediate value between that in the two references, $\gamma_{\rm i} = 0.02$. The boundary conditions for the equivalent flux are available for electron energy transport by changing $\langle v_{\rm e}\rangle$ to $\langle \varepsilon_{\rm e} v_{\rm e}\rangle$ and taking a mean energy, $\varepsilon_0 = 1$ eV, for secondary electrons emitted at the cathode surface, even if in the literature the given energy values are between 2 and 6 eV [33]. For all surfaces, the normal ion flux is given by $\Gamma_{\rm i}^{\perp} = n_{\rm i} v_{\rm thi}/4 + \delta\mu_{\rm i} n_{\rm i} E_{\rm eff}^{\perp}$, where $v_{\rm thi}$ is the ion thermal velocity; $\delta = 1$ if $E_{\rm eff}^{\perp}$ is directed to the surface and $\delta = 0$ otherwise. For the Poisson equation, the boundary conditions include the fact that the anode is grounded ($V_{\rm anode} = 0$) and that a negative voltage, $V_{\rm cathode}$, is applied to the cathode. For symmetry reasons at the reactor axis $\partial V/\partial r = 0$, and for the particle density $\partial n_{\rm s}/\partial r = 0$, s = e, i.

6. Numerical solution

As was already mentioned above, due to cylindrical symmetry of the magnetron, a bi-dimensional (r, z) treatment is complete for a proper description of the discharge. Even if an electronic azimuthal flux exists, it can be expressed in the (r, z) co-ordinate system as shown in equation (7*b*). For the charged particles, continuity type equations,

$$\frac{\partial n_{\rm s}}{\partial t} + \left[\frac{1}{r}\frac{\partial}{\partial r}(r\Gamma_{{\rm s}r}) + \frac{\partial}{\partial z}(\Gamma_{{\rm s}z})\right] = S, \qquad {\rm s} = {\rm e, i}, \quad (19)$$

have to be solved. The transport equation for electron energy has the same form, if we replace the particle density by the electron mean energy density and express the source term S_ε correctly. In equation (19) the fluxes of the charged species must be introduced in order to obtain the particle densities. If the expression for the global flux for electrons (5) and ions (12) is used, it will result in a complicated system to be solved. Two conditions are imposed to simplify the problem: (i) the fluxes are expressed in the forms (4) and (13) and (ii) only the drift–diffusion component of the flux is kept in the left-hand side terms of equation (19). The latter condition does not affect the ion equation, because in expression (13) the flux already has a classical drift–diffusion form. Under these assumptions, equation (19) are developed as

$$\frac{n_{\rm e}^{t+\Delta t} - n_{\rm e}^{t}}{\Delta t} + \left[\frac{1}{r}\frac{\partial}{\partial r}(r\Gamma_{er}^{0}) + \frac{\partial}{\partial z}(\Gamma_{ez}^{0})\right]^{t+\Delta t} = S^t - \left[\frac{1}{r}\frac{\partial}{\partial r}(r\Gamma_{er}^{1}) + \frac{\partial}{\partial z}(\Gamma_{ez}^{1})\right]^{t}, \qquad (20a)$$

$$\frac{n_{\rm i}^{t+\Delta t} - n_{\rm i}^{t}}{\Delta t} + \left[\frac{1}{r}\frac{\partial}{\partial r}(r\Gamma_{ir}) + \frac{\partial}{\partial z}(\Gamma_{iz})\right]^{t+\Delta t} = S^t, \qquad (20b)$$

which gives a semi-implicit temporal discretization scheme, where Δt is the time step. The spatial discretization method is based on the finite difference scheme. The equations (20*a*) and (20*b*) are multiplied by $r\,{\rm d}r\,{\rm d}z$ and are integrated over a grid cell, thus allowing us to avoid the singularity problem of the divergence for $r = 0$. The drift–diffusion fluxes for electrons and ions are discretized using the Scharfetter–Gummel exponential scheme [34]. Equations (20*a*) and (20*b*) can then be solved to obtain particle densities and drift–diffusion fluxes. After that, $\vec{\Gamma}_{\rm e}^{1}$ is deduced from equation (7*a*) and the total electron flux is obtained. The plasma potential is calculated from the Poisson equation for every time step. All equations are numerically solved using a band matrix method [35], including the boundary conditions.

The time step value is constrained by the convergence of the numerical methods used to solve the system of equations mentioned above. First of all, the Courant–Friedrichs–Lewy (CFL) stability criterion [36, 37] must be satisfied. This criterion imposes the condition that a particle can cover at most the dimension of one cell per time step. Also, for the stability of the space charge and electric field, the time step must have an upper limit equal to the Maxwell relaxation time [37].

7. Results

Typical simulation results for the whole volume of the discharge are presented for argon at a pressure $p = 20$ mTorr, neutral temperature $T_{\rm Ar} = 350$ K and a polarization of the cathode of -550 V. The spatial distribution of the potential in the reactor is plotted in figure 3. In the largest part of the discharge, the plasma potential is weakly positive. The cathode fall thickness is about 5 mm on the magnetron axis while in the highest confinement zone it does not exceed 3.8 mm. This zone corresponds to the region where the vectors $\vec{E}$ and $\vec{B}$ are perpendicular to each other. As the electric field is axially dominant in the cathode fall, the magnetic field must be radial and, according to figure 2, this occurs in front of the cathode at a radius of about 9.5 mm. The confinement zone is visible in figure 3, being characterized by a higher local potential, but is more evident in figure 4 where we obtain the electron and ion densities. The representation is bi-dimensional (r, z), but rotating the picture around the z-axis, according to the cylindrical symmetry, it is clearly shown that the negative glow in the magnetron is a torus. The maximum

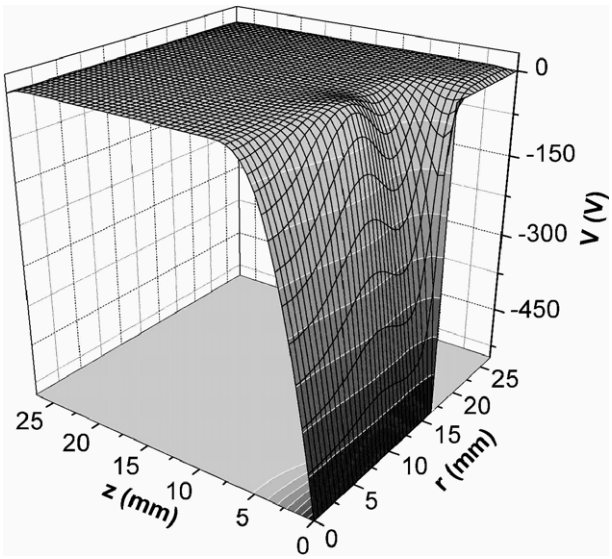

Figure 3. Plasma potential distribution.

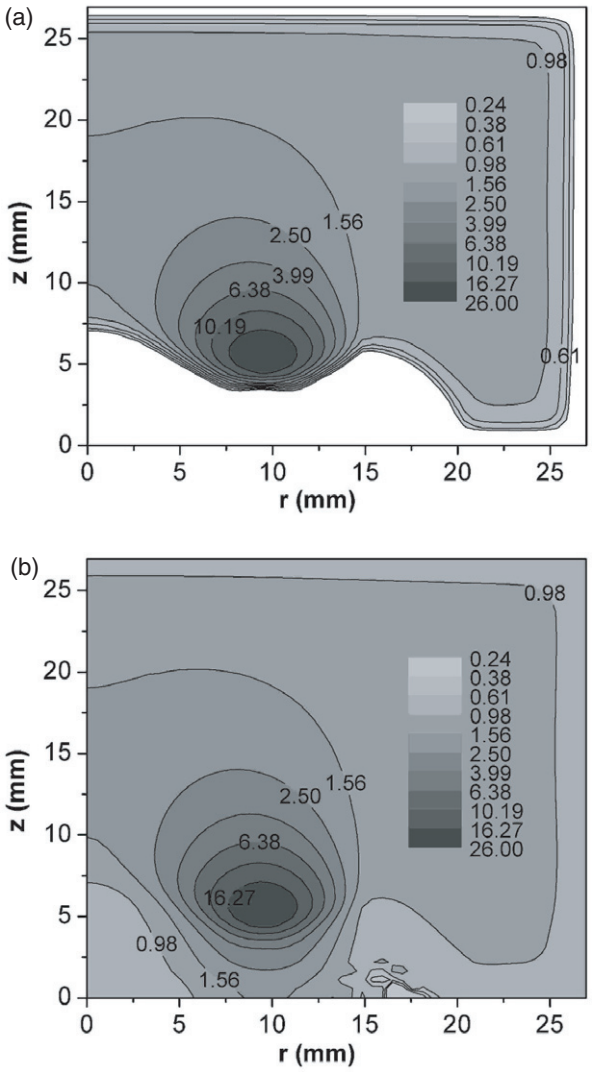

Figure 4. Electron (*a*) and ion (*b*) map densities (10^9 cm^{-3}).

density both for electrons and ions reaches 2.5×10^{10} cm^{-3} at $r = 9.35$ mm, $z = 5.5$ mm. The electron density decreases significantly in the anode sheath and cathode fall with respect to the volume, the white zone in figure 4(*a*) corresponding to a density lower than 2.4×10^8 cm^{-3}. The ion density has the same comportment, but its drop is less important, especially in the cathode fall. For better visualization, in figure 5 we plot the axial dependence of the electron and ion densities for two different radial positions: on the discharge axis ($r = 0$) and in the region of maximum density of the plasma torus ($r = 9.35$ mm). Both figures show a quasi-neutral plasma in the volume of the discharge, with a density of about 1.5×10^9 cm^{-3}; the quasi-neutrality is strongly perturbed in front of the electrodes where ion sheaths appear. In the cathode fall the ion sheath is formed due to the negative voltage applied on the cathode. At the anode, due to its extended surface, there is significant electron loss and the ions remain dominant in the sheath. Thus, the plasma potential becomes positive with respect to the grounded anode (figure 3), in accordance with the measurements in [9]. The shapes of the plasma potential and charged particle densities in figures 3–5 are in very good agreement with previous results from the hybrid model [1, 14], the latter having the same spatial profile mentioned above. Comparable results are given also by PIC simulation [11–13], even if they are performed for a different geometry. In figure 6 we give the axial ion particle flux in the cathode fall. While the ion energy at the target does not depend on the radial position r, the particle flux is a measure of the sputtering profile of the cathode. It must be mentioned that, unlike figures 2–4, this picture is plotted in a reduced region in front of the cathode, $r_{max} = 16.5$ mm, $z_{max} = 10$ mm, where the ion flux is really interesting. Positive/negative values of the ion flux denote the orientation from/towards the cathode of the flux vector. Plotting data were not limited to the cathode fall ($z \leqslant 5$ mm) to show also the positive diffusive flux due to the ion density gradient.

In order to study the influence of the gas pressure on the discharge, in figure 7 we show the axial distribution of the plasma potential, electron density and electron mean energy at the radial position $r = 9.35$ mm, for $V_{cathode} = -350$ V, $T_{Ar} = 350$ K and $p = 5, 10, 20$ and 30 mTorr. These results are in good agreement with the spatial dependence of the plasma parameters obtained under similar conditions from Langmuir probe measurements [38]. In the volume of the discharge, the plasma potential is practically constant at a positive value and it decreases with increasing pressure (figure 7(*a*)). This is strongly correlated with the electron mean energy, which shows the same evolution with pressure (figure 7(*c*)). The plasma potential, V_p, creates a trap for the electrons with energies lower than eV_p. These electrons are thermalized in the volume and they have Maxwellian distribution functions even if the pressure is low [9]. On the other hand, energy losses for electrons are more important at high pressure and in this case the electron mean energy diminishes. As a consequence, the potential V_p necessary to trap these electrons also diminishes. The density of the electron energy, $\langle n_e \varepsilon_e \rangle$, is calculated from equation (1*c*) of the fluid model. The electron mean energy, ε_e, is obtained by dividing $\langle n_e \varepsilon_e \rangle$ by the electron density. The latter is very low in the cathode fall ($\sim 10^6$ cm^{-3}) and this can lead to an overestimation of the electron mean energy. For this reason,

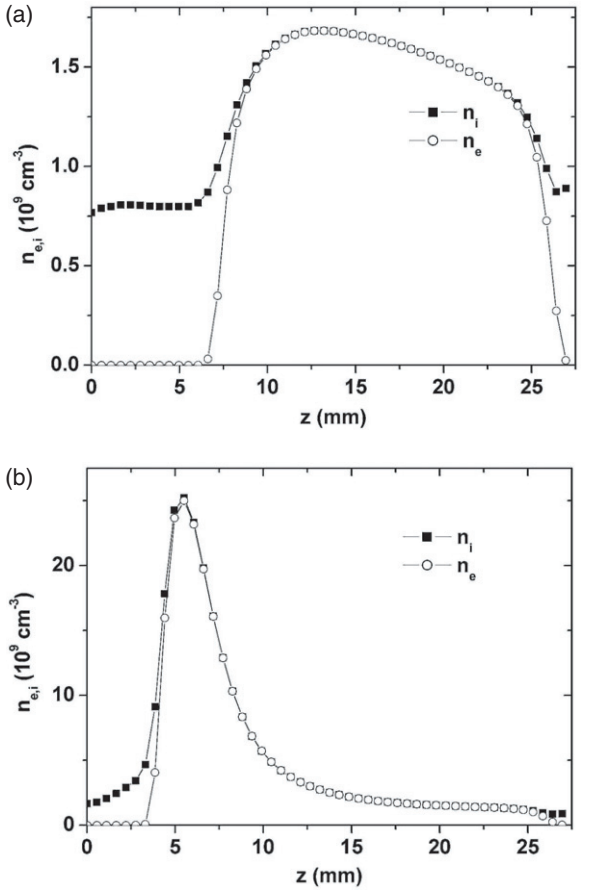

Figure 5. Axial distribution of electron and ion densities at two radial positions: (*a*) $r = 0$; (*b*) $r = 9.35$ mm.

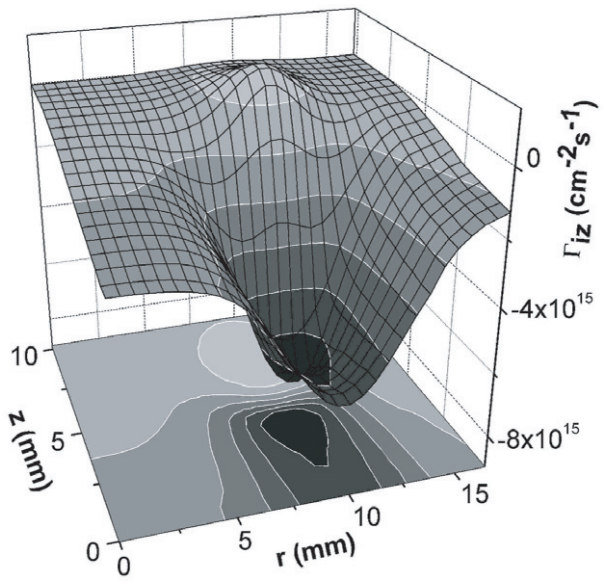

Figure 6. Axial ionic particle flux in the cathode fall.

the energy axis was cut off at the entrance in the cathode fall in figure 7(*c*). The thickness of the cathode fall also diminishes with increasing pressure, as can be seen both in figures 7(*a*) and (*b*). For high pressure (which means high plasma density) a potential drop can be observed behind the plasma torus and, implicitly, a field reversal. This can be caused by a higher loss rate of the electron energy at the end of the cathode fall which generates a minimum in the mean energy of the electrons. This leads to an accumulation of electrons in that region, which reduces the value of the local potential.

Examining the results in figures 7(*b*) and (*c*), the validity of the Maxwellian EEDF approach must be discussed. Most of the measurements of EEDF in magnetrons report bi-Maxwellian distributions [9, 39–42], with two groups of hot and cold electrons, at 2–7 cm from the cathode. In the plasma torus only hot electrons are reported while cold electrons are dominant far from the cathode (>7–8 cm). In [39] the authors found that 'inside the confined plasma region only single gradient semi-logarithmic plots were obtained, implying Maxwellian electrons of a well defined single temperature. Any energetic, 'beam-like' electrons accelerated directly through the cathode sheath superimposed on the thermal bulk electrons could not be detected. Outside the closed fields lines, however, two electron temperatures were obtained, with a hot component with a concentration less than 10% that of the cold group'. Their findings are in line with those of [40]. In our case, due to the high density of the charged particles in the plasma torus ($\sim 10^{10}$ cm^{-3}), the assumption of a Maxwellian distribution function for electrons in this region is reasonable. Taking into account the short linear dimension of our modelled reactor ($\sim$2.7 cm), it can be supposed that only one group of electrons is present in the whole volume. Hot electrons are rapidly lost at the anode while only cold electrons with mean energy below eV_p remain thermalized in the potential trap, as already discussed. Even if the assumption of a Maxwellian EEDF is only a first approximation for the fluid model described in this paper, our results correspond with the measurements in [38], where the electrons are treated as one group and only one electron temperature is reported.

Figure 7(*b*) shows that the gas pressure strongly influences the density of the plasma torus, but not that of the volume plasma. The axial distribution of electron density at $r = 0$, which is representative of the volume plasma, shows a very weak dependence on pressure. This can be explained by taking into account the fact that the ionization frequency depends both on the gas density and electron energy. In the range of energy that characterizes the volume plasma (below 8 eV), the ionization frequency is very low, as also the influence of the pressure. Things are different in the plasma torus where electron energies exceed the ionization threshold for argon. In this region, the gas pressure has more influence than the electron energy. For more relevance, the maximum of the electron density in the plasma torus is plotted against the pressure in figure 8, for two different cathode voltages, −350 and −550 V. The plasma density increases both with pressure and cathode voltage.

8. Concluding remarks

An original method of treating the fluid equations is proposed in this paper. Separating the electron flux into two parts and treating the influence of the magnetic field as an additional term in the flux expression seems to be a valid and convenient approach. The plasma potential, charged particle densities and ion flux at the cathode are shown as representative results. Our

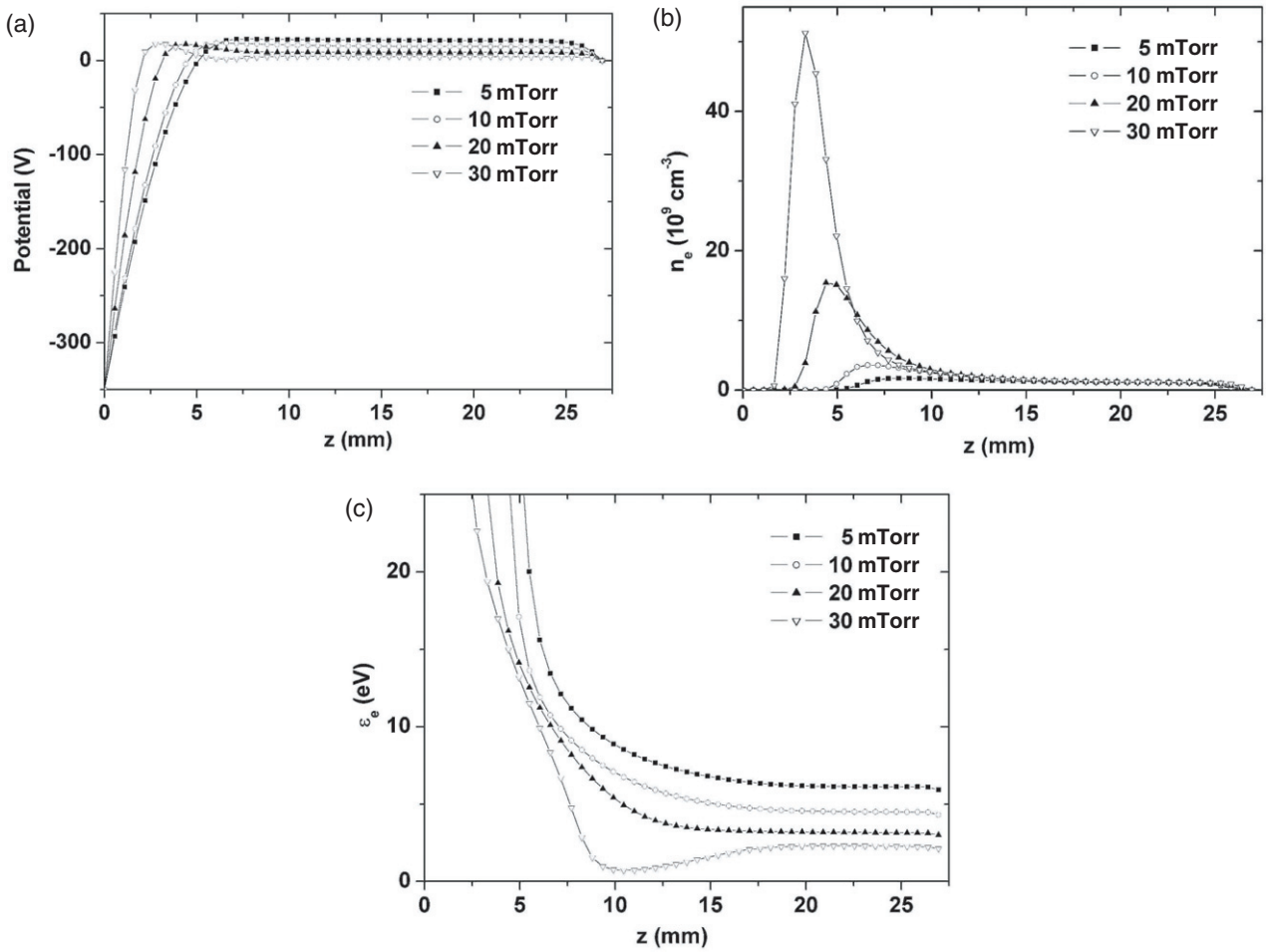

Figure 7. Axial distribution of plasma potential (*a*), electron density (*b*) and electron mean energy (*c*) at $r = 9.35$ mm, for $V_{\text{cathode}} = -350$ V, $T_{\text{Ar}} = 350$ K and $p = 5$, 10, 20 and 30 mTorr.

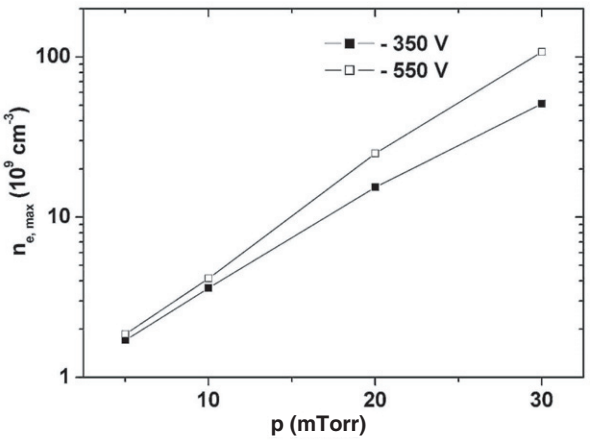

Figure 8. Maximum of the electron density as a function of pressure, for $V_{\text{cathode}} = -350$ and -550 V.

calculations are in good agreement with previous ones obtained by PIC or hybrid schemes. The variation of the plasma parameters (potential, electron density, electron mean energy) with the gas pressure corresponds to the experimental results reported by other authors. Even more, if this approach works for a term containing a vector product, $\vec{v}_e \times \vec{B}$, which creates a strong coupling between the flux components, Γ_{er}, $\Gamma_{e\varphi}$, Γ_{ez}, it is expected to work all the better for the other terms neglected in equation (1*b*). Thus, we can consider the electron inertial term, pressure anisotropy or the contribution of the finite fraction $f_{\text{iz}}/f_{\text{me}}$ to the total electron flux. Each term can be introduced following the same procedure presented in this paper, the advantage being that we obtain an easy method for linearizing and solving equations (1*a*) and (1*c*) by keeping in the left-hand side term only a drift–diffusive flux form. Such approaches, which solve time-dependent fluid equations, can be used for RF magnetron discharges without modifications except for the applied potential at the cathode.

Acknowledgments

C Costin would like to thank the French Government for his PhD fellowship at Laboratoire de Physique des Gaz et des Plasmas. We are also grateful to Dr T Minea for very helpful discussions. This work was partly supported by CNCSIS Romania, grant A/1344/2003.

References

[1] Shidoji E, Ando E and Makabe T 2001 *Plasma Sources Sci. Technol.* **8** 621

[2] Kouznetsov V, Macak K, Schneider J M, Helmersson U and Petrov I 1999 *Surf. Coat. Technol.* **122** 290
[3] Gudmundsson J T, Alami J and Helmersson U 2001 *Appl. Phys. Lett*. **78** 3427
[4] Ehiasarian A P, New R, Munz W-D, Hultman L, Helmersson U and Kouznetsov V 2002 *Vacuum* **65** 147
[5] Bruckner W, Kaltofen R, Thomas J, Hecker M, Uhlemann M, Oswald S, Elefant D and Schneider C M 2003 *J. Appl. Phys*. **94** 4853
[6] Lee J, Kim J H and Im S 2003 *Appl. Phys. Lett*. **83** 2689
[7] Snyders R, Wautelet M, Gouttebaron R, Dauchot J P and Hecq M 2003 *Surf. Coat. Technol*. **174** 1282
[8] Debal F, Wautelet M, Bretagne J, Dauchot J P and Hecq M 2000 *Plasma Sources Sci. Technol*. **9** 152
[9] Mihaila I, Popa G, Anita V, Costin C, Sirghi L and Turcu I 2002 *Le Vide - Science, Technique Appl.* **57** 316 (in French)
[10] Minea T M, Bretagne J, Gousset G, Magne L, Pagnon D and Touzeau M 1999 *Surf. Coat. Technol*. **116** 558
Minea T M, Bretagne J and Gousset G 1999 *IEEE Trans. Plasma Sci.* **27** 94
[11] Shon C H and Lee J K 2002 *Appl. Surf. Sci*. **192** 258
[12] Kondo S and Nanbu K 2001 *J. Vac. Sci. Technol.* A **19** 830
Kondo S and Nanbu K 2001 *J. Vac. Sci. Technol.* A **19** 838
[13] Nanbu K, Segawa S and Kondo S 1996 *Vacuum* **47** 1013
Nanbu K and Kondo S 1997 *Japan. J. Appl. Phys.* **36** 4808
[14] Shidoji E, Ohtake H, Nakano N and Makabe T 1999 *Japan. J. Appl. Phys.* **38** 2131
Shidoji E, Nakano N and Makabe T 1999 *Thin Solid Films* **351** 37
Shidoji E, Ness K and Makabe T 2001 *Vaccum* **60** 299
Shidoji E and Makabe T 2003 *Thin Solid Films* **442** 27
[15] Hagelaar G J M, Bareilles J, Garrigues L and Bœuf J-P 2002 *J. Appl. Phys*. **91** 5592
Garrigues L, Bareilles J, Bœuf J-P and Boyd I D 2002 *J. Appl. Phys*. **91** 9521
Hagelaar G J M, Bareilles J, Garrigues L and Bœuf J-P 2003 *J. Appl. Phys*. **93** 67
[16] Porokhova I A, Golubovskii Yu B, Bretagne J, Tichy M and Benkhe J F 2001 *Phys. Rev.* E **63** 56408
Porokhova I A, Golubovskii Yu B, Holik M, Kudrna P, Tichy M, Wilke C and Behnke J F 2003 *Phys. Rev.* E **68** 16401
[17] White R D, Robson R E and Ness K F 2001 *J. Phys. D: Appl. Phys.* **34** 2205
[18] Trennepohl W Jr, Bretagne J, Gousset G, Pagnon D and Touzeau M 1996 *Plasma Sources Sci. Technol*. **5** 607
[19] Debal F, Bretagne J, Dauchot J P, Hecq M and Wautelet M 2001 *Plasma Sources Sci. Technol*. **10** 30
[20] Cramer N F 1997 *J. Phys. D: Appl. Phys.* **30** 2573
[21] Bradley J W and Lister G 1997 *Plasma Sources Sci. Technol.* **6** 524
Bradley J W 1998 *Plasma Sources Sci. Technol*. **7** 572
[22] Minea T 1999 *PhD Thesis* Université Paris-Sud XI Orsay, p 14 (in French)
[23] Rossnagel S M and Kaufman H R 1987 *J. Vac. Sci. Technol.* A **5** 88
[24] Alves L L, Gousset G and Ferreira C M 1997 *Phys. Rev.* E **55** 890
Alves L L, Gousset G and Vallee S 2003 *IEEE Trans. Plasma Sci*. **31** 572
[25] Bretagne J, Callede G, Legentil M and Puech V 1986 *J. Phys. D: Appl. Phys.* **19** 761
[26] Richards A D, Thompson B E and Sawin H H 1987 *Appl. Phys. Lett*. **50** 492
[27] Salabas A, Gousset G and Alves L L 2002 *Plasma Sources Sci. Technol*. **11** 448
[28] Ellis H W, Pai R Y, McDaniel E W, Mason E A and Viehland L A 1976 *Atomic Data Nucl. Data Tables* **17** 177
[29] Phelps A V 1991 *J. Phys. Chem. Ref. Data* **20** 557
[30] Buyle G, De Bosscher W, Depla D, Eufinger K, Haemers J and De Gryse R 2003 *Vacuum* **70** 29
[31] Phelps A V and Petrovic Z Lj 1999 *Plasma Sources Sci. Technol*. **8** R21
[32] Auday G, Guillot P, Galy J and Brunet H 1998 *J. Appl. Phys*. **83** 5917
[33] Chapman B 1980 *Glow Discharge Processes* (New York: Wiley) p 91
[34] Scharfetter D L and Gummel H K 1969 *IEEE Trans. Electron Devices* **16** 64
[35] Press W H, Teukolsky S A, Vetterling W T and Flannery B P 1992 *Numerical Recipes in Fortran. The Art of Scientific Computing* 2nd edn (Cambridge: Cambridge University Press)
[36] Courant R, Friedrichs K O and Lewy H 1967 *IBM J.* **11** 215
[37] Barnes M S, Colter T J and Elta M E 1987 *J. Appl. Phys.* **61** 81
[38] Rossnagel S M and Kaufman H R 1986 *J. Vac. Sci. Technol.* A **4** 1822
[39] Bradley J W, Thompson S and Aranda Gonzalvo Y 2001 *Plasma Sources Sci. Technol*. **10** 490
[40] Sheridan T E, Goeckner M J and Goree J 1991 *J. Vac. Sci. Technol.* A **9** 688
[41] Spatenka P, Vlcek J and Blazek J 1999 *Vacuum* **55** 165
[42] Seo S-H, In J-H and Chang H-Y 2004 *Plasma Sources Sci. Technol.* **13** 409